CrossMark

ORIGINAL PAPER

Dynamic characteristics of flexible rotor with squeeze film damper excited by two frequencies

Huizheng Chen · Lei Hou · Yushu Chen · Rui Yang

Abstract This paper is focused on the dynamic characteristics of a flexible rotor with squeeze film damper excited by two frequencies. The multiple harmonic balance method and Runge–Kutta method are combined to analyze the periodic solution and quasi-periodic solution of the system. The nonlinear characteristics discussed are fastened on the resonance region corresponding, respectively, to the rigid body translation mode and first bending mode. In the former region, the motion of disk center shows the 'hard spring' characteristic, and the combination frequencies are dominated by the difference between double low excitation frequency and high excitation frequency and the difference between double high excitation frequency and low excitation frequency. In the latter region, however, the combination frequencies are dominated by the difference between high excitation frequency and double low excitation frequency and the difference between triple low excitation frequency and double high excitation frequency. Moreover, the motion of disk center shows a kind of 'cross', 'soft spring' or 'hard spring' characteristics with the variation of the ratio of the two excitation frequencies. Besides, the independent quasi-periodic solution coexists with the periodic solution in these cases. The system is sensitive to the ratio of excitation frequencies, and it could have two independent quasi-periodic solutions in some conditions. The results in this paper provide a reveal of nonlinear characteristics in this type of double excitation nonlinear rotor system.

Keywords Two-frequency excitation · Squeeze film damper · Nonlinear characteristic · Jump phenomenon · Unstable solution · Quasi-periodic motion

1 Introduction

Squeeze film dampers (SFDs) are simple configurations mounted on aircraft engines to suppress vibrations of rotors and promote system stability. The system with SFDs is nonlinear, which means the nonlinear forces caused by oil film will lead to undesired unbalance responses in some operation conditions. These nonlinear characteristics of squeeze film damper have provided plenty of material for research since Cooper's work in 1963 [1], and many researchers reported jump phenomenon and non-synchronous motion in SFD-rotor system by theoretical analysis [2–4] and experimental validation [5,6]. Furthermore, sub-harmonic motions, which contain fractional frequency components in system responses, were observed by Holmes et al. [7–9] in their experimental works.

With the appearance of more detailed research work based on different computational methods, more non-

H. Chen · L. Hou · Y. Chen · R. Yang
School of Astronautics, Harbin Institute of Technology,
Harbin 150001, People's Republic of China

L. Hou (✉)
School of Energy Science and Engineering, Harbin Institute
of Technology, Harbin 150001, People's Republic of China
e-mail: houlei@hit.edu.cn

linear characters alternating with parameters variation are revealed. Zhao [10,11] used the trigonometric collocation method embedding arc-length continuation algorithm to investigate the stability and bifurcation of an eccentric SFD-rotor system, in which the period motion, sub-harmonic motion and quasi-periodic motion transforming into each other with the variation of rotor speed were observed, and these results were compared with those of a concentric system. Zhu [12] compared the slow acceleration method with synchronous circular centered-orbit motion solution and numerical integration method in the study of a flexible rotor supported by SFDs, in which three forms of the multiple-solution responses due to saddle-node bifurcation were obtained. Sundararajan [13] presented a shooting scheme along with arc-length continuation algorithm for periodically forced rotor systems, as an example, an eccentric SFD system was solved by this method. Besides, the similar results to Zhao's work [11], this system exists another multiple-solution range, in which a stable period-3 solution coexists with a period-1 solution. Furthermore, the system has the evolution route: period-3, period-6, chaos, period-3, with rotor speed running up. Based on a numerical continuation method, Inayat-Hussain [14,15] also obtained a period-3 motion which coexists with a chaotic motion due to period-doubling bifurcation in a rigid rotor supported by SFDs without centering springs. This period-3 motion has two evolution routes to chaos: period-doubling bifurcation and boundary crisis. Comparing with the preceding results in SFDs without centering springs, the system supported by centering springs has the following two routes to chaos: period-doubling cascades and type 3 intermittency. Bonello [16] presented an integrated approach containing receptance harmonic balance method and time marching techniques to analyze the period solution and aperiodic solution of a multiple SFDs system, in which the sub-harmonic motion and quasi-period motion were verified by simulations and experiments. In conclusion, since each single method has its advantage and drawback, the development of hybrid method is a general tendency applied to reveal more detailed characteristics of nonlinear system.

Similar to the research works of SFDs with simple structure, complex nonlinear dynamic behaviors also have been found in some other SFDs with sophisticated structure. In the study of a porous squeeze film damper system lubricated by micropolar fluid, Cai-Wan [17]

showed the wide ranges of quasi-period motion and chaotic motion with varying rotor speed. In rotor systems with full-floating ring bearings, containing two serial SFDs separated by a rotatable floating ring, the undesired symmetry-breaking effect and total instability phenomenon caused by self-excited vibrations were reported by Schweizer [18]. Further, the sub-synchronous oscillations and the critical limit cycle were reported in the semi-floating ring bearings [19], the floating ring of which is not rotatable. Zhou [20] analyzed the nonlinear responses of rotor with ball bearing and floating ring squeeze film dampers by discussing the effects of out-ring mass, bearing stiffness and supports stiffness on the non-synchronous response, and it was concluded that the floating ring SFD can effectively prevent bistable responses of the system.

All these research works mentioned above focus on the responses with a single-frequency excitation. However, there remains a need for the studies of responses caused by two-frequency excitations which comes from dual-rotor systems such as aircraft engines. To simulate on a twin-spool aero-engine system with a real size, Bonello and Pham [21,22] introduced the impulsive receptance method (IRM) and compared it with reformulation of the Newmark-beta method and receptance harmonic balance method (RHBM) in order to choose proper methods for analyzing large-order nonlinear systems. Furthermore, these selected methods [23] were used to achieve an insight into the effect of the ratio between two rotor's speeds on the vibration response. It was shown that the responses are particularly sensitive to the initial phase angle between the rotors, especially when the speed ratio was a ratio of two low integers. Obviously, affected by two unbalanced excitations of different frequencies, a nonlinear system shows some interesting complex characteristics which need to be investigated in detail.

The motivation of this paper is to detect the nonlinear characteristics of a flexible rotor supported by squeeze film damper excited by two different frequencies. By using harmonic balance method matching fourth Runge–Kutta method and Hsu method, the periodic solutions containing combined frequencies and quasi-period solutions are obtained, and stability of the periodic solutions affected by parameters, such as ratio of excitation frequencies, oil viscosity and clearance, are also analyzed.

2 Model of SFD-rotor system

As outlined in Fig. 1, the low-pressure rotor of aircraft engine is simplified as an asymmetric, linear-elastic rotor, the left end is supported by a SFD in parallel with linear spring, and the right end is supported by a linear spring. The dotted line disk represents a simplified high-pressure rotor, which provides a high-frequency excitation to the system. The rotor model is comprised of a disk of mass m_o, left journal of mass m_a, right journal of mass m_b and massless flexible shaft. The left journal is supported by a linear spring of stiffness k_a and a SFD of clearance c. The right journal is supported by a linear spring of stiffness k_b. Hence, considering the short bearing approximation of oil film [12], the motion equations of the rotor system can be written as:

$$
\begin{cases}
m_o\ddot{x} + c_1(\dot{x} - \dot{x}_1) - c_2(\dot{\theta}_y - \dot{\theta}_{y1}) + k_{rr}(x - x_1) \\
\quad - k_{r\varphi}(\theta_y - \theta_{y1}) = \delta_1\Omega_1^2\cos\Omega_1 t + \delta_2\Omega_2^2\cos\Omega_2 t \\
m_o\ddot{y} + c_1(\dot{y} - \dot{y}_1) + c_2(\dot{\theta}_x - \dot{\theta}_{x1}) + k_{rr}(y - y_1) \\
\quad + k_{r\varphi}(\theta_x - \theta_{x1}) = \delta_1\Omega_1^2\sin\Omega_1 t + \delta_2\Omega_2^2\sin\Omega_2 t \\
J_d\ddot{\theta}_x + J_p\Omega_1\dot{\theta}_y + c_3(\dot{y} - \dot{y}_1) + c_4(\dot{\theta}_x - \dot{\theta}_{x1}) \\
\quad + k_{\varphi r}(y - y_1) + k_{\varphi\varphi}(\theta_x - \theta_{x1}) = \delta_2\Omega_2^2 l_3\sin\Omega_2 t \\
J_d\ddot{\theta}_y - J_p\Omega_1\dot{\theta}_x - c_3(\dot{x} - \dot{x}_1) + c_4(\dot{\theta}_y - \dot{\theta}_{y1}) \\
\quad - k_{\varphi r}(x - x_1) + k_{\varphi\varphi}(\theta_y - \theta_{y1}) = -\delta_2\Omega_2^2 l_3\cos\Omega_2 t \\
m_a\ddot{x}_a - \gamma_2 c_1(\dot{x} - \dot{x}_1) + \gamma_2 c_2(\dot{\theta}_y - \dot{\theta}_{y1}) - \gamma_2 k_{rr}(x - x_1) \\
\quad + \gamma_2 k_{r\varphi}(\theta_y - \theta_{y1}) + c_5\dot{x}_a + k_a x_a + F_{cx} = 0 \\
m_a\ddot{y}_a - \gamma_2 c_1(\dot{y} - \dot{y}_1) - \gamma_2 c_2(\dot{\theta}_x - \dot{\theta}_{x1}) - \gamma_2 k_{rr}(y - y_1) \\
\quad - \gamma_2 k_{r\varphi}(\theta_x - \theta_{x1}) + c_5\dot{y}_a + k_a y_a + F_{cy} = 0 \\
m_b\ddot{x}_b - \gamma_1 c_1(\dot{x} - \dot{x}_1) + \gamma_1 c_2(\dot{\theta}_y - \dot{\theta}_{y1}) - \gamma_1 k_{rr}(x - x_1) \\
\quad + \gamma_1 k_{r\varphi}(\theta_y - \theta_{y1}) + c_6\dot{x}_b + k_b x_b = 0 \\
m_b\ddot{y}_b - \gamma_1 c_1(\dot{y} - \dot{y}_1) - \gamma_1 c_2(\dot{\theta}_x - \dot{\theta}_{x1}) - \gamma_1 k_{rr}(y - y_1) \\
\quad - \gamma_1 k_{r\varphi}(\theta_x - \theta_{x1}) + c_6\dot{y}_b + k_b y_b = 0
\end{cases}
\tag{1}
$$

in which, $l = l_1 + l_2$, $\gamma_1 = l_1/l$ and $\gamma_2 = l_2/l$ are used to define the length and ratio parameters, $x_1 = \gamma_2 x_a + \gamma_1 x_b$, $y_1 = \gamma_2 y_a + \gamma_1 y_b$, $\theta_{x1} = (y_a - y_b)/l$ and $\theta_{y1} = (x_b - x_a)/l$ are rigid body displacements of disk center, k_{rr}, $k_{r\varphi}$ and $k_{\varphi\varphi}$ represent stiffness parameters of the shaft, $c_1 \sim c_6$ represent damper parameters, J_p and J_d represent polar moment of inertia and equatorial moment of inertia, δ_1 and δ_2 are equivalent unbalance values, ω_1 and ω_2 are rotational speeds of low-pressure rotor and high-pressure rotor, $F_{cx} = F_r x_a/r - F_\tau y_a/r$ and $F_{cy} = F_r y_a/r + F_\tau x_a/r$ are components of oil film force in x-coordinate and y-

coordinate, $F_r = \mu R L^3/c^3\left(I_3^{02}\dot{r} + I_3^{11}r\dot{\psi}\right)$ and $F_\tau = \mu R L^3/c^3\left(I_3^{11}\dot{r} + I_3^{20}r\dot{\psi}\right)$ are the oil film forces of radial direction and tangential direction, $r = \sqrt{x_a^2 + y_a^2}$ and $\psi = \arctan(y_a/x_a)$ are the displacements of radial direction and tangential direction, μ is the viscosity coefficient of oil, R is the radius of journal, L is the length of SFD, and the integral parameters are defined as $I_n^{lm} = \int_{\theta_1}^{\theta_2}\frac{\sin^l\theta\cos^m\theta d\theta}{(1+r\cos\theta/c)^n}$ [24].

The dimensionless parameters are introduced as follows:

$$
\tau = \Omega_1 t, \quad q_1 = \frac{x}{c}, \quad q_2 = \frac{y}{c}, \quad q_3 = \frac{\theta_x l}{c},
$$

$$
q_4 = \frac{\theta_y l}{c}, q_5 = \frac{x_a}{c}, \quad q_6 = \frac{y_a}{c}, \quad q_7 = \frac{x_b}{c}, \quad q_8 = \frac{y_b}{c}.
$$

Thus, the motion equation (1) can be rewritten as:

$$
\begin{cases}
q_1'' + \zeta_1 q_1' - \zeta_2 q_4' - (\zeta_2 + \zeta_1\gamma_2)q_5' \\
\quad + (\zeta_2 - \gamma_1\zeta_1)q_7' + \kappa_1 q_1 - \kappa_2 q_4 - (\kappa_2 + \kappa_1\gamma_2)q_5 \\
\quad + (\kappa_2 - \gamma_1\kappa_1)q_7 = U_1\cos\tau + \xi^2 U_2\cos\xi\tau \\
q_2'' + \zeta_1 q_2' + \zeta_2 q_3' - (\zeta_2 + \zeta_1\gamma_2)q_6' \\
\quad + (\zeta_2 - \gamma_1\zeta_1)q_8' + \kappa_1 q_2 + \kappa_2 q_3 - (\kappa_2 + \kappa_1\gamma_2)q_6 \\
\quad + (\kappa_2 - \gamma_1\kappa_1)q_8 = U_1\sin\tau + \xi^2 U_2\sin\xi\tau \\
\alpha_0 q_3'' + \alpha_0\eta q_4' + \zeta_3 q_2' + \zeta_4 q_3' - (\zeta_4 + \zeta_3\gamma_2)q_6' \\
\quad + (\zeta_4 - \gamma_1\zeta_3)q_8' + \kappa_3 q_2 + \kappa_4 q_3 - (\kappa_4 + \kappa_3\gamma_2)q_6 \\
\quad + (\kappa_4 - \gamma_1\kappa_3)q_8 = \xi^2 U_3\sin\xi\tau \\
\alpha_0 q_4'' - \alpha_0\eta q_3' - \zeta_3 q_1' + \zeta_4 q_4' + (\zeta_4 + \zeta_3\gamma_2)q_5' \\
\quad - (\zeta_4 - \gamma_1\zeta_3)q_7' - \kappa_3 q_1 + \kappa_4 q_4 + (\kappa_4 + \kappa_3\gamma_2)q_5 \\
\quad - (\kappa_4 - \gamma_1\kappa_3)q_7 = -\xi^2 U_3\cos\xi\tau \\
\alpha_1 q_5'' - \gamma_2\zeta_1 q_1' + \gamma_2\zeta_2 q_4' + \gamma_2(\zeta_2 + \gamma_2\zeta_1)q_5' \\
\quad - \gamma_2(\zeta_2 - \gamma_1\zeta_1)q_7' + \zeta_5 q_5' - \gamma_2\kappa_1 q_1 + \gamma_2\kappa_2 q_4 \\
\quad + \gamma_2(\kappa_2 + \gamma_2\kappa_1)q_5 - \gamma_2(\kappa_2 - \gamma_1\kappa_1)q_7 + \kappa_5 q_5 \\
\quad + B\bar{F}_{cx} = 0 \\
\alpha_1 q_6'' - \gamma_2\zeta_1 q_2' - \gamma_2\zeta_2 q_3' + \gamma_2(\zeta_2 + \gamma_2\zeta_1)q_6' \\
\quad - \gamma_2(\zeta_2 - \gamma_1\zeta_1)q_8' + \zeta_5 q_6' - \gamma_2\kappa_1 q_2 - \gamma_2\kappa_2 q_3 \\
\quad + \gamma_2(\kappa_2 + \gamma_2\kappa_1)q_6 - \gamma_2(\kappa_2 - \gamma_1\kappa_1)q_8 + \kappa_5 q_6 \\
\quad + B\bar{F}_{cy} = 0 \\
\alpha_2 q_7'' - \gamma_1\zeta_1 q_1' + \gamma_1\zeta_2 q_4' + \gamma_1(\zeta_2 + \gamma_2\zeta_1)q_5' \\
\quad - \gamma_1(\zeta_2 - \zeta_1\gamma_1)q_7' + \zeta_6 q_7' - \gamma_1\kappa_1 q_1 + \gamma_1\kappa_2 q_4 \\
\quad + \gamma_1(\kappa_2 + \gamma_2\kappa_1)q_5 - \gamma_1(\kappa_2 - \kappa_1\gamma_1)q_7 \\
\quad + \kappa_6 q_7 = 0 \\
\alpha_2 q_8'' - \gamma_1\zeta_1 q_2' - \gamma_1\zeta_2 q_3' + \gamma_1(\zeta_2 + \gamma_2\zeta_1)q_6' \\
\quad - \gamma_1(\zeta_2 - \zeta_1\gamma_1)q_8' + \zeta_6 q_8' - \gamma_1\kappa_1 q_2 - \gamma_1\kappa_2 q_3 \\
\quad + \gamma_1(\kappa_2 + \gamma_2\kappa_1)q_6 - \gamma_1(\kappa_2 - \kappa_1\gamma_1)q_8 + \kappa_6 q_8 = 0
\end{cases}
\tag{2}
$$

in which, the other dimensionless parameters are defined as: $\zeta_1 = \frac{c_1}{m_o\Omega_1}$, $\zeta_2 = \frac{c_2}{m_o l\Omega_1}$, $\zeta_3 = \frac{c_3}{m_o l\Omega_1}$,

Fig. 1 Simplified model of low-pressure rotor
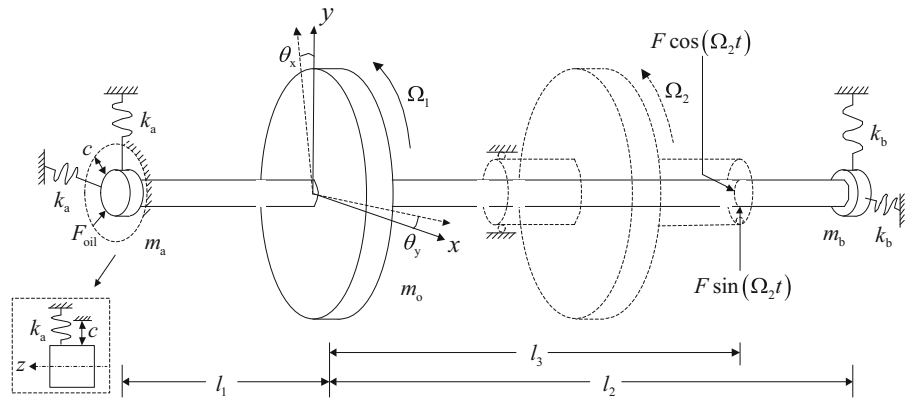
$\zeta_4 = \frac{c_4}{m_o l^2 \Omega_1}$, $\zeta_5 = \frac{c_5}{m_o \Omega_1}$, $\zeta_6 = \frac{c_6}{m_o \Omega_1}$, $\kappa_1 = \frac{k_{rr}}{m_o \Omega_1^2}$,
$\kappa_2 = \frac{k_{r\varphi}}{m_o l \Omega_1^2}$, $\kappa_3 = \frac{k_{r\varphi}}{m_o l \Omega_1^2}$, $\kappa_4 = \frac{k_{\varphi\varphi}}{m_o l^2 \Omega_1^2}$, $\kappa_5 = \frac{k_a}{m_o \Omega_1^2}$,
$\kappa_6 = \frac{k_b}{m_o \Omega_1^2}$, $\eta = \frac{J_p}{J_d}$, $\alpha_0 = \frac{J_d}{m_o l^2}$, $\alpha_1 = \frac{m_a}{m_o}$, $\alpha_2 = \frac{m_b}{m_o}$,
$U_1 = \frac{\delta_1}{cm_o}$, $U_2 = \frac{\delta_2}{cm_o}$, $U_3 = \frac{\delta_2 l_3}{m_o lc}$, $\xi = \frac{\Omega_2}{\Omega_1}$, $\varepsilon = \frac{r}{c}$,
$B = \frac{\mu R L^3}{m_o c^3 \Omega_1}$, $\bar{F}_{cx} = \bar{F}_r \frac{q_5}{\varepsilon} - \bar{F}_\tau \frac{q_6}{\varepsilon}$, $\bar{F}_{cy} = \bar{F}_r \frac{q_6}{\varepsilon} + \bar{F}_\tau \frac{q_5}{\varepsilon}$,
$\bar{F}_r = I_3^{02} \varepsilon' + I_3^{11} \varepsilon \psi'$, $\bar{F}_\tau = I_3^{11} \varepsilon' + I_3^{20} \varepsilon \psi'$.

3 Method of solution and stability analysis

3.1 Multiple harmonic balance method

Equation (2) describes a nonlinear system with external two-frequency excitations, in which the responses may contain two incommensurable frequencies and a series of combination frequencies of them. To analyze the system with multiple-frequency excitation, a multiple harmonic balance method proposed by Kim [25] in a study on internal resonance problem of incommensurable frequencies is chosen. The discrete time solution of Eq. (2) can be assumed as:

$$q_j(m, n) = \sum_{k=-M}^{M} \sum_{l=-M}^{M} a_{j,k,l} \cos \frac{2\pi}{N}(mk + nl)$$
$$+ b_{j,k,l} \sin \frac{2\pi}{N}(mk + nl)$$
$$= \sum_{k=-M}^{M} \sum_{l=-M}^{M} a_{j,k,l} \cos(k\tau_1 + l\tau_2)$$
$$+ b_{j,k,l} \sin(k\tau_1 + l\tau_2) \quad (3)$$

The substitution variables $\tau_1 = \tau$, $\tau_2 = \xi\tau$ represent independent time dimension, both of them vary from 0 to 2π, and m, n varying from 0 to $N - 1$.

Correspondingly, the nonlinear forces are expressed as:

$$\begin{cases} \bar{F}_{cx}(q_5, q_6, q_5', q_6')(m, n) = \sum_{k=-M}^{M} \sum_{l=-M}^{M} \\ \times \left(c_{5,k,l} \cos \frac{2\pi}{N}(mk + nl) + d_{5,k,l} \sin \frac{2\pi}{N}(mk + nl) \right) \\ \bar{F}_{cy}(q_5, q_6, q_5', q_6')(m, n) = \sum_{k=-M}^{M} \sum_{l=-M}^{M} \\ \times \left(c_{6,k,l} \cos \frac{2\pi}{N}(mk + nl) + d_{6,k,l} \sin \frac{2\pi}{N}(mk + nl) \right) \end{cases}$$
(4)

Substituting Eqs. (3) and (4) into Eq. (2), and considering the differential operator $\frac{d}{d\tau} = \frac{\partial}{\partial\tau_1} + \xi \frac{\partial}{\partial\tau_2}$, rearranging the terms with the same trigonometric elements leads to the following equations:

$$g_{1,k,l} = \left[\kappa_1 - (k + l\xi)^2\right] a_{1kl} + \zeta_1 (k + l\xi) b_{1kl}$$
$$- \kappa_2 a_{4kl} - \zeta_2 (k + l\xi) b_{4kl} - (\kappa_2 + \gamma_2 \kappa_1) a_{5kl}$$
$$- (\zeta_2 + \gamma_2 \zeta_1)(k + l\xi) b_{5kl} + (\kappa_2 - \gamma_1 \kappa_1) a_{7kl}$$
$$+ (\zeta_2 - \gamma_1 \zeta_1)(k + l\xi) b_{7kl} - U_1 \phi_1 - \xi^2 U_2 \phi_2 = 0$$
$$g_{2,k,l} = -\zeta_1 (k + l\xi) a_{1kl} + \left[\kappa_1 - (k + l\xi)^2\right] b_{1kl}$$
$$+ \zeta_2 (k + l\xi) a_{4kl} - \kappa_2 b_{4kl} + (\zeta_2 + \gamma_2 \zeta_1)$$
$$(k + l\xi) a_{5kl} - (\kappa_2 + \gamma_2 \kappa_1) b_{5kl} - (\zeta_2 - \gamma_1 \zeta_1)$$
$$(k + l\xi) a_{7kl} + (\kappa_2 - \gamma_1 \kappa_1) b_{7kl} = 0$$
$$\vdots$$
$$g_{15,k,l} = -\gamma_1 \zeta_1 (k + l\xi) b_{2kl} - \gamma_1 \kappa_2 a_{3kl}$$
$$- \gamma_1 \zeta_2 (k + l\xi) b_{3kl} + \gamma_1 (\kappa_2 + \gamma_2 \kappa_1) a_{6kl}$$
$$+ \gamma_1 (\zeta_2 + \gamma_2 \zeta_1)(k + l\xi) b_{6kl} - \gamma_1 \kappa_1 a_{2kl}$$
$$+ \left[(\kappa_6 - \gamma_1 \kappa_2 + \gamma_1^2 \kappa_1) - \alpha_2 (k + l\xi)^2\right] a_{8kl}$$
$$+ \left[\gamma_1 (\gamma_1 \zeta_1 - \zeta_2) + \zeta_6\right](k + l\xi) b_{8kl} = 0$$

$$g_{16,k,l} = \gamma_1 (\kappa_2 + \gamma_2 \kappa_1) b_{6kl}$$
$$+ \left[(\kappa_6 - \gamma_1 \kappa_2 + \gamma_1^2 \kappa_1) - \alpha_2 (k + l\xi)^2 \right] b_{8kl}$$
$$- \left[\gamma_1 (\gamma_1 \zeta_1 - \zeta_2) + \zeta_6 \right] (k + l\xi) a_{8kl}$$
$$\gamma_1 \zeta_1 (k + l\xi) a_{2kl} - \gamma_1 \kappa_1 b_{2kl} + \gamma_1 \zeta_2 (k + l\xi) a_{3kl}$$
$$- \gamma_1 \kappa_2 b_{3kl} - \gamma_1 (\zeta_2 + \gamma_2 \zeta_1)(k + l\xi) a_{6kl} = 0$$
$$(5)$$

in which, $\phi_1 = \begin{cases} 1 & (k=1, l=0) \\ 0 & \text{others} \end{cases}$, $\phi_2 = \begin{cases} 1 & (k=0, l=1) \\ 0 & \text{others} \end{cases}$,

the other terms are shown in Appendix 2. Equation (5) can be expressed as:

$$G(P, Q) = [g_{1,k,l}(P, Q), g_{2,k,l}(P, Q),$$
$$\dots, g_{16,k,l}(P, Q)]^{\mathrm{T}} = 0 \quad (6)$$

$$\begin{bmatrix} P \\ Q \end{bmatrix}^{\mathrm{T}} = \begin{bmatrix} a_{1,k,l} \ b_{1,k,l} \ a_{2,k,l} \ b_{2,k,l} \ \dots \ a_{8,k,l} \ b_{8,k,l} \\ c_{1,k,l} \ d_{1,k,l} \ c_{2,k,l} \ d_{2,k,l} \ \dots \ c_{8,k,l} \ d_{8,k,l} \end{bmatrix}^{\mathrm{T}}$$
$$(7)$$

Equation (6) contains a series of algebraic equations about unknown coefficients P and Q. The coefficients Q can be expressed by using the coefficients P by Eq. (3) and the relationships as follows:

$$\begin{bmatrix} c_{5,k,l} \\ c_{6,k,l} \end{bmatrix} = \frac{2}{N^2} \sum_{m=0}^{N-1} \sum_{n=0}^{N-1} \begin{bmatrix} \bar{F}_{cx}(q_5, q_6, q_5', q_6')(m, n) \\ \bar{F}_{cy}(q_5, q_6, q_5', q_6')(m, n) \end{bmatrix}$$
$$\times \cos \frac{2\pi}{N}(mk + nl)$$

$$\begin{bmatrix} d_{5,k,l} \\ d_{6,k,l} \end{bmatrix} = \frac{2}{N^2} \sum_{m=0}^{N-1} \sum_{n=0}^{N-1} \begin{bmatrix} \bar{F}_{cx}(q_5, q_6, q_5', q_6')(m, n) \\ \bar{F}_{cy}(q_5, q_6, q_5', q_6')(m, n) \end{bmatrix}$$
$$\times \sin \frac{2\pi}{N}(mk + nl) \quad (8)$$

Finally, Eq. (6) only contains unknown coefficients P which can be solved by iterative method such as Newton-Rapson algorithm:

Table 1 Parameters of rotor and squeeze film damper system

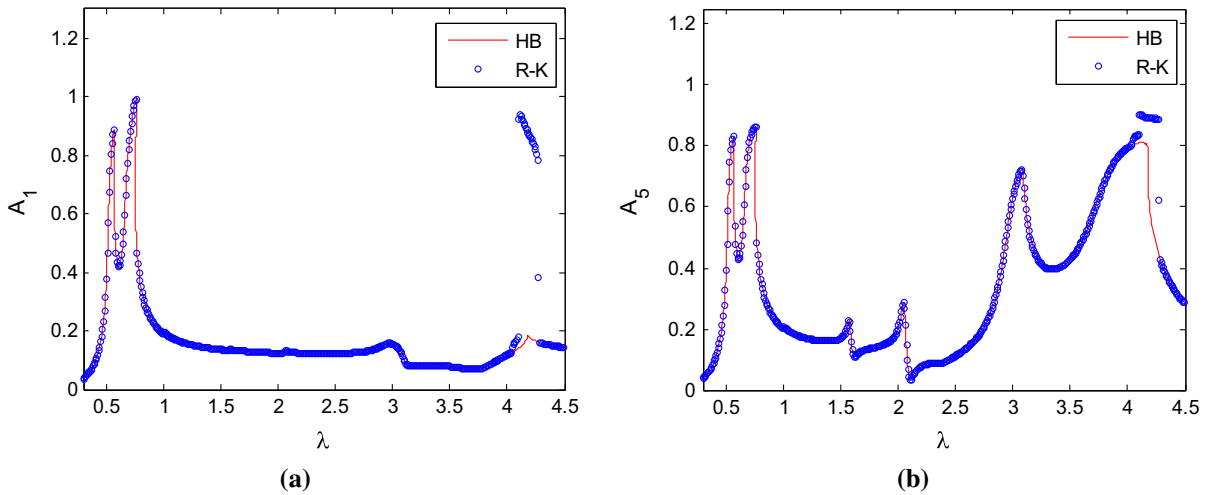| Mass (kg)	Stiffness (N/m)	Damping (Ns/m)	SFD parameters	Other parameters
$m_o = 120$	$k_{rr} = 2.66 \times 10^7$	$c_1 = 266$	$c = 0.20$ mm	$l_1 = 0.8$ m
$m_a = 12$	$k_{r\varphi} = k_{\varphi r} = 9.96 \times 10^6$	$c_2 = c_3 = 99.6$	$L = 15$ mm	$l_2 = 1.25$ m
$m_b = 18$	$k_{rr} = 2.21 \times 10^7$	$c_4 = 221$	$R = 39.5$ mm	$l_3 = 0.5$ m
	$k_a = 3.6 \times 10^6$	$c_5 = 36$	$\mu = 1.562 \times 10^{-2}$ Ns/m^2	$J_d = 2.5$ kgm^2
	$k_b = 7.2 \times 10^6$	$c_6 = 72$		$J_p = 5.0$ kgm^2
				$\delta_1 = 170 \times 10^{-5}$ kgm
				$\delta_2 = 140 \times 10^{-5}$ kgm

Fig. 2 Frequency–Amplitude results of two numerical algorithms ($\xi = 1.30$). **a** center of disk q_1, **b** journal of SFD q_5

$$J^{(i)} \left(P^{(i+1)} - P^{(i)} \right) + G^{(i)} = 0 \qquad (9)$$

The Jacobian matrix is expressed as:

$$J = \frac{dG(P, Q)}{dP} = \frac{\partial G(P, Q)}{\partial P} + \frac{\partial G(P, Q)}{\partial Q} \cdot \frac{dQ}{dP}$$
$$(10)$$

Based on the relationships of P and Q which revealed in Eqs. (3) and (8), term $\frac{dQ}{dP}$ can be derived. Therefore, by giving an proper initial value $P^{(0)}$, the convergence solution can be obtained.

3.2 Pseudo-arc-length continuation

Generally, the convergence of Newton-Rapson algorithm depends on the selection of initial value, the improper initial value will lead to faults of the algorithm, especially at the neighborhood of some bifurcation points such as saddle-node bifurcation points [26]. To overcome the limitation of the algorithm, a pseudo-arc-length continuation is embedded in the Newton-Rapson algorithm as follows:

$$\begin{cases} \frac{\partial G}{\partial P} \frac{dP}{ds} + \frac{\partial G}{\partial \lambda} \frac{d\lambda}{ds} = 0 \\ \frac{dP^T}{ds} \frac{dP}{ds} + \left(\frac{d\lambda}{ds} \right)^2 = 1 \end{cases} \qquad (11)$$

in which, $\lambda = \frac{\Omega_1}{\Omega_0}$ is a variable of frequency, Ω_0 is a constant selected for convenience. The new initial value can be estimated by:

$$\left[P^{(1)} \ \lambda^{(1)} \right]^T = \left[P^{(0)} \ \lambda^{(0)} \right]^T + \delta \left[\frac{dP}{ds} \ \frac{d\lambda}{ds} \right]^T \qquad (12)$$

where

$$\begin{cases} \frac{dP_i}{ds} = (-1)^i C(P, \lambda) \cdot \det \left[DH_{[-i]}(P, \lambda) \right] \\ \frac{d\lambda}{ds} = (-1)^{N+1} C(P, \lambda) \cdot \det \left[DH_{[-(N+1)]}(P, \lambda) \right] \end{cases}$$
$$(13)$$

$$DH(P, \lambda) = \left[\frac{\partial G}{\partial P} \ \frac{\partial G}{\partial \lambda} \right] \qquad (14)$$
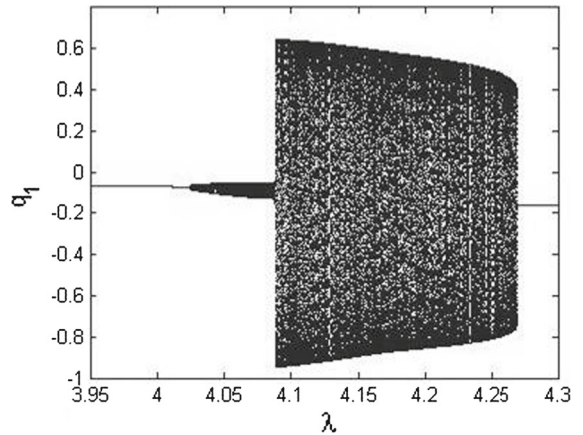

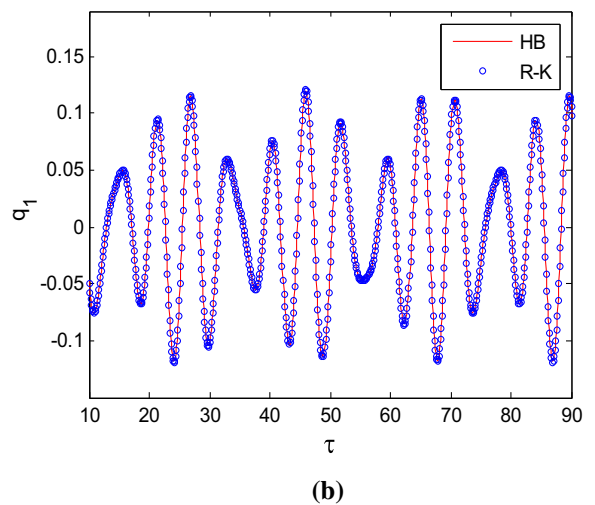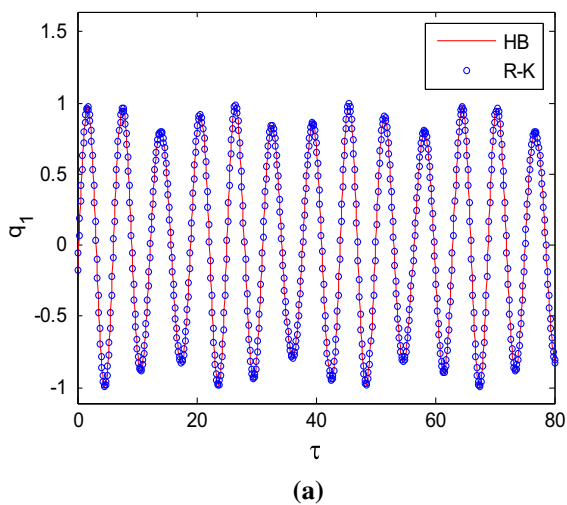**Fig. 4** Bifurcation diagram of center of disk q_1

Fig. 3 Time responses of q_1 in different resonance region. **a** $\lambda = 0.762$, **b** $\lambda = 4.013$

$$C\left(P,\lambda\right)=\frac{(-1)^{N+1}\,\mathrm{sgn}\left[G_P\left(P^{(0)},\lambda^{(0)}\right)\right]}{\sqrt{\sum_{i=1}^{N+1}\left(\det\left[DH_{[-i]}\right]\right)^2}} \quad (15)$$

in which, the operator notation $DH_{[-i]}$ means matrix DH subtract by the i throw.

According to the new initial value $\left[\,P^{(1)}\,\,\lambda^{(1)}\,\right]^{\mathrm{T}}$, the solution can be obtained by the iterative formula derived from Eq. (11) as follows:

$$\begin{bmatrix} P^{(i+1)} \\ \lambda^{(i+1)} \end{bmatrix} = \begin{bmatrix} P^{(i)} \\ \lambda^{(i)} \end{bmatrix} - \begin{bmatrix} G_P\left(P^{(i)},\lambda^{(i)}\right) & G_\lambda\left(P^{(i)},\lambda^{(i)}\right) \\ \frac{dP^T}{ds} & \frac{d\lambda}{ds} \end{bmatrix}^{-1}$$

$$\cdot \begin{bmatrix} G\left(P^{(i)},\lambda^{(i)}\right) \\ \frac{dP^T}{ds}\left(P^{(i)}-P^{(1)}\right)+\frac{d\lambda}{ds}\left(\lambda^{(i)}-\lambda^{(1)}\right) \end{bmatrix}. \quad (16)$$

3.3 Floquet stability analysis and Hsu's method

The Floquet multipliers are useful indexes to reflect the stability of the system. If all the Floquet multipliers are within the unit circle in the complex plane, the period solution is stable, or else the period solution is unstable. There are three ways that a periodic solution loses stability [13]:
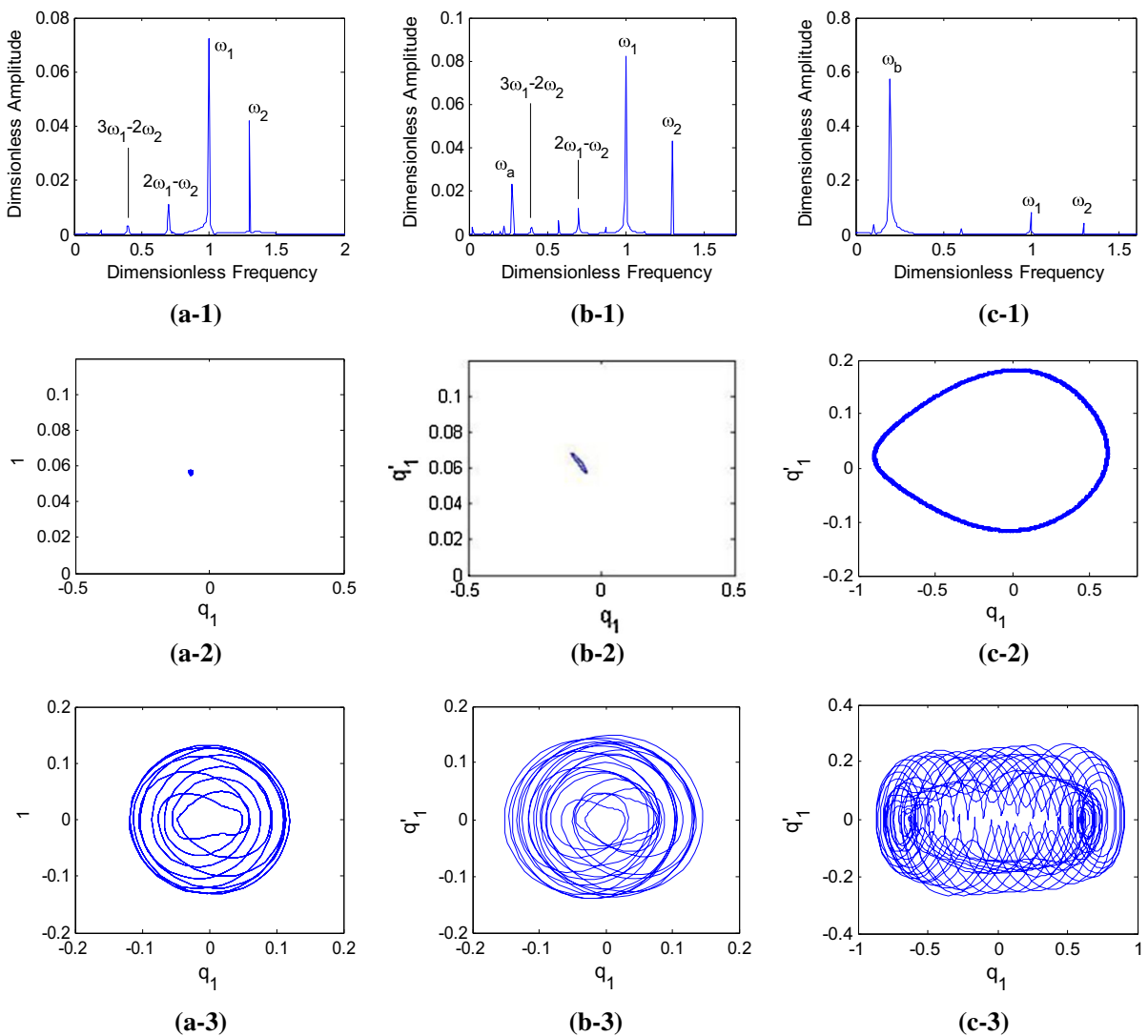

Fig. 5 Frequency spectrogram, Poincare section and phase diagram of three different frequencies. **a** $\lambda = 4.01$, **b** $\lambda = 4.053$, **c** $\lambda = 4.147$

(1) One of the multipliers cross the unit circle through $(+1, 0)$, the period solution loses stability by saddle-node bifurcation, or pitchfork bifurcation or symmetry-breaking bifurcation.

(2) One of the multipliers cross the unit circle through $(-1, 0)$, the period solution loses stability by period-doubling bifurcation.

(3) A pair of conjugate multipliers cross the unit circle, the period solution loses stability by secondary Hopf bifurcation.

Hsu [27] proposed a numerical scheme to obtain Floquet multipliers, which is carried out by discretizing one period into a number of intervals and multiplying constant coefficient matrices over each interval one by one. This scheme is used here, and its procedures are list as follows:

Firstly, rewrite the motion Eq. (2) into the state equation:

$$U = \begin{bmatrix} q_1 \ q_1' \cdots q_8 \ q_8' \end{bmatrix}^{\mathrm{T}} \tag{17}$$

$$U'\left(\hat{\tau}\right) = F\left(U\right) \tag{18}$$

Then, deduce the perturbation equation about ΔU:

$$\left(U^*\left(\hat{\tau}\right) + \Delta U\right)' = F\left(\hat{\tau}, U^*\left(\hat{\tau}\right) + \Delta U\right) \tag{19}$$

$$
\Delta U' = \left.\frac{\partial F\left(\hat{\tau}, U\left(\hat{\tau}\right)\right)}{\partial U\left(\hat{\tau}\right)}\right|_{U=U^*}
$$
$$
\cdot \Delta U = A\left(\hat{\tau}, U^*\left(\hat{\tau}\right)\right)\Delta U \tag{20}
$$

where $U^*\left(\hat{\tau}\right)$ is the period solution, thus matrix A is a period matrix.

Finally, compute monodromy matrix D:

$$
D = \prod_{n=N}^{1} \exp\left(\Delta T \cdot A\left(U^*\left(\hat{\tau}_n\right), \hat{\tau}_n\right)\right)
$$
$$
\approx \prod_{n=N}^{1}\left(I + \sum_{j}^{N_j}\frac{\left(\Delta T \cdot A\left(U^*\left(\hat{\tau}_n\right), \hat{\tau}_n\right)\right)^j}{j!}\right) \tag{21}
$$

in which $\Delta T = T/N$ represents the time interval, $\hat{\tau}_n$ represents the end time of n th interval.

The eigenvalues of monodromy matrix D are the Floquet multipliers of the corresponding periodic solution.

4 Results and discussions

The numerical analysis is carried out by using both harmonic balance method and fourth order Runge-Kutta method. The physical parameters of the system are listed in Table 1.

4.1 Period solution and quasi-periodic solution

Choosing the maximal harmonic parameter $M = 5$ and constant frequency $\Omega_0 = 300$ rad/s, the relationships between dimensionless amplitude and dimensionless
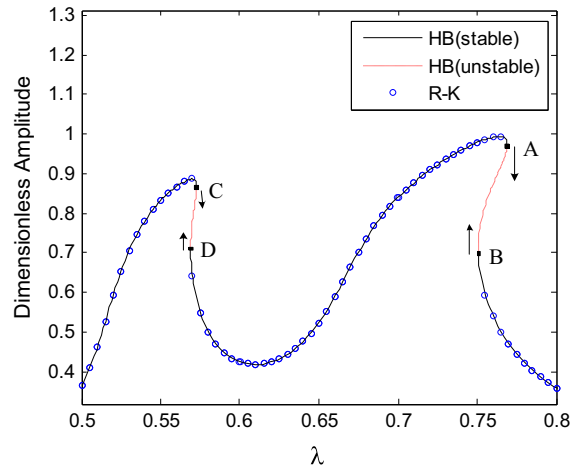

Fig. 6 Frequency–Amplitude curves of resonance region of the rigid body translation

Table 2 Floquet multipliers nearby bifurcation point

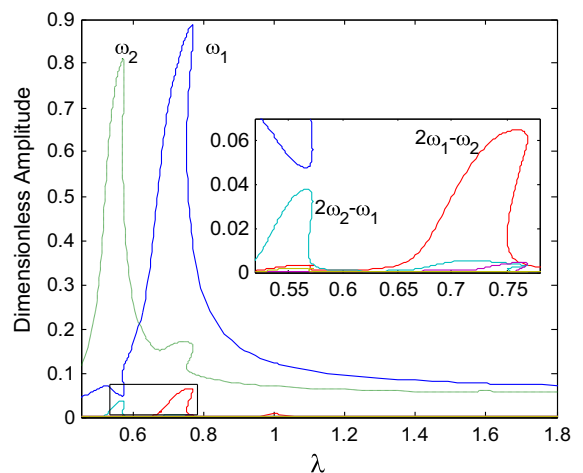| Point	λ	Floquet multiplier
A	$0.7690 \rightarrow 0.7691$	$0.9564 \rightarrow 1.0476$
B	$0.7508 \rightarrow 0.7509$	$1.0683 \rightarrow 0.7311$
C	$0.5728 \rightarrow 0.5729$	$0.9404 \rightarrow 1.0162$
D	$0.5690 \rightarrow 0.5691$	$1.1690 \rightarrow 0.9805$

Fig. 7 Amplitude curves for different response frequency components

frequency are shown in Fig. 2. It is clear that there are three pairs of resonant peaks in Fig. 2b from low frequency to high frequency, which are, respectively, cor-
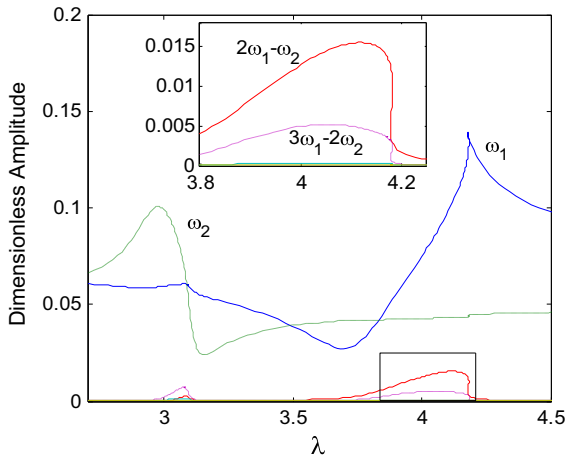
responding to the vibration modes of rigid body translation and rigid body rotation, and the first bending mode. Each pair of peaks represents the resonant peaks excited by low-frequency ω_1 and high-frequency ω_2. The influence on the rigid body rotation is not obvious in Fig. 2a. Thus, the nonlinear characteristics of system are concentrated on the rigid body translation mode and the first bending mode. Moreover, the solutions from the harmonic balance method agree well with that from the Runge-Kutta method in most of the frequency region. The displacement responses of q_1 on two frequencies of resonant peaks $\lambda = 0.762$ and $\lambda = 4.013$ are shown in Fig. 3, which means the choice of harmonic parameter is applicable.

Besides, there is a region that two results are not fit nearby $\lambda = 4.2$. To explain the difference, the bifurcation diagram between $\lambda = 3.95$ and $\lambda = 4.30$ is shown in Fig. 4. Since there are two periods 2π and $2\pi/\xi$ in this two-frequency excited system, the period $2\nu\pi$ is chosen as the period of Poincare mapping to ensure the correctness of calculation. The integer ν

Fig. 8 Amplitude curves for different response frequency components

Fig. 9 Frequency–amplitude curves of resonance region of first bending mode ($\xi = 1.3$)
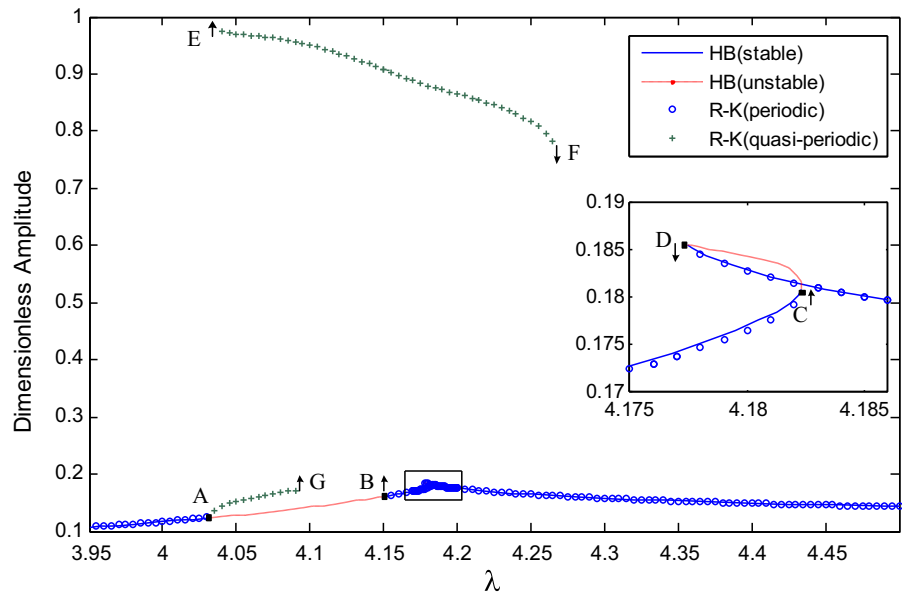
Table 3 Floquet multipliers nearby bifurcation point

Point	λ	Floquet multiplier
A	$4.0386 \rightarrow 4.0476$	$0.0743 \pm 0.9944\,\mathrm{i} \rightarrow 0.0638 \pm 1.0031\,\mathrm{i}$
B	$4.1470 \rightarrow 4.1512$	$-0.3296 \pm 0.9475\,\mathrm{i} \rightarrow -0.3662 \pm 0.9253\,\mathrm{i}$
C	$4.1823 \rightarrow 4.1821$	$0.9827 \rightarrow 1.0414$
D	$4.1776 \rightarrow 4.1775$	$1.0633 \rightarrow 0.9779$

should satisfy the condition that $\xi\nu$ is an integer, thus the period $2\nu\pi$ can be a common period of the two excitations. Based on this definition, the meaning of Poincare section needs to be redefined: a single point means the periodic solutions contain all $k\omega_1 + l\omega_2$ frequencies, some independent points mean the solutions contain fractional ratio of $k\omega_1 + l\omega_2$ frequencies, and a closed circle means that there is a quasi-periodic solution which belongs to neither $k\omega_1 + l\omega_2$ nor their fractional ratio. It is clear to see the system gets into aperiodic motion at $\lambda = 4.02$, and the amplitude of the motion increase dramatically at $\lambda = 4.089$, finally at $\lambda = 4.27$, the motion returns back to periodic solution. The frequency spectrogram, Poincare section and phase diagram corresponding to the three motions are given in Fig. 5. In the case of $\lambda = 4.01$, the motion of the system is periodic, and the major response frequencies are dimensionless excitation frequencies $\omega_1 = 1.00$, $\omega_2 = 1.30$ and their combined frequencies $2\omega_1 - \omega_2 = 0.70$, $3\omega_1 - 2\omega_2 = 0.40$. In the case of $\lambda = 4.053$, besides the frequencies ω_1, ω_2 and their combined frequencies, there is a frequency $\omega_a = 0.275$, which cannot be expressed as integral

multiple combination of ω_1 and ω_2. The amplitude of ω_a is lower than that of ω_1 and ω_2, and the system motion is quasi-periodic motion with a low amplitude. Different from the former two, in the case of $\lambda = 4.147$, the dominating frequencies are no longer ω_1 and ω_2, but a new frequency $\omega_b = 0.195$, which differs from ω_a and also cannot be expressed as integral multiple combination of excitation frequencies. And, the motion of system is a quasi-periodic motion with high amplitude, and a jump phenomenon, harmful to the safety of the system, occurs when the frequency λ increases. The difference of results obtained by harmonic balance method and Runge–Kutta method reflects the limitation of the harmonic balance method: since the frequency of quasi-periodic solution cannot be expressed by the assumptive frequencies $k\omega_1 + l\omega_2$, the difference of magnitude is caused by the amplitude value of quasi-periodic frequency component ω_a in Fig. 5(b-1) and ω_b in Fig. 5(c-1). More discussions about the relationship between periodic solution and quasi-periodic solution will be given in Sect. 4.3 in this paper.
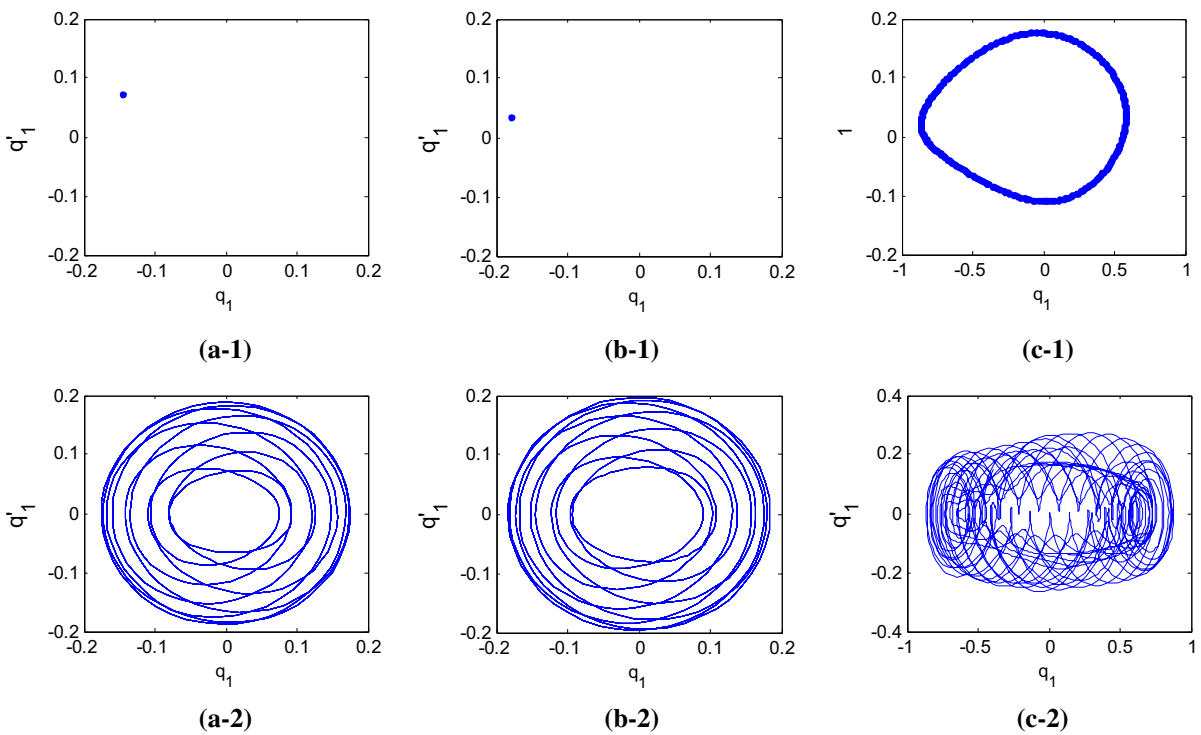

Fig. 10 Poincare sections and phase diagrams of two periodic solutions and a quasi-periodic solution at $\lambda = 4.179$ ($\xi = 1.3$)

4.2 Resonance region of rigid body translation mode

As mentioned before, the resonance of the rigid body translation is a region where the response amplitude is large and the nonlinear characteristic is outstanding. In Fig. 6, the two resonant peaks from left to right are corresponding to the primary resonant peaks caused by the high excitation frequency ω_2 and the low excitation frequency ω_1 respectively. The dotted line represents the unstable solution, and points A, B, C, D are saddle–node bifurcation points judged by Floquet multiplier, as listed in Table 2. The jump phenomenon will occur when the rotor speed goes up through point A, C or goes down through point B, D. The result is similar to that of rotor-SFD system with single excitation frequency [12]. Besides this nonlinear characteristic, the responses of the system also contain components of the two excitation frequencies and their combined frequencies, as shown in Fig. 7. It is clear to see that there are two dominating frequencies ω_1 and ω_2, corresponding to the two resonant peaks. When λ runs near 0.55, the resonant peak is aroused by the excitation of higher-frequency ω_2, and with the increase in the frequency ω_2, the amplitude of frequency component ω_1
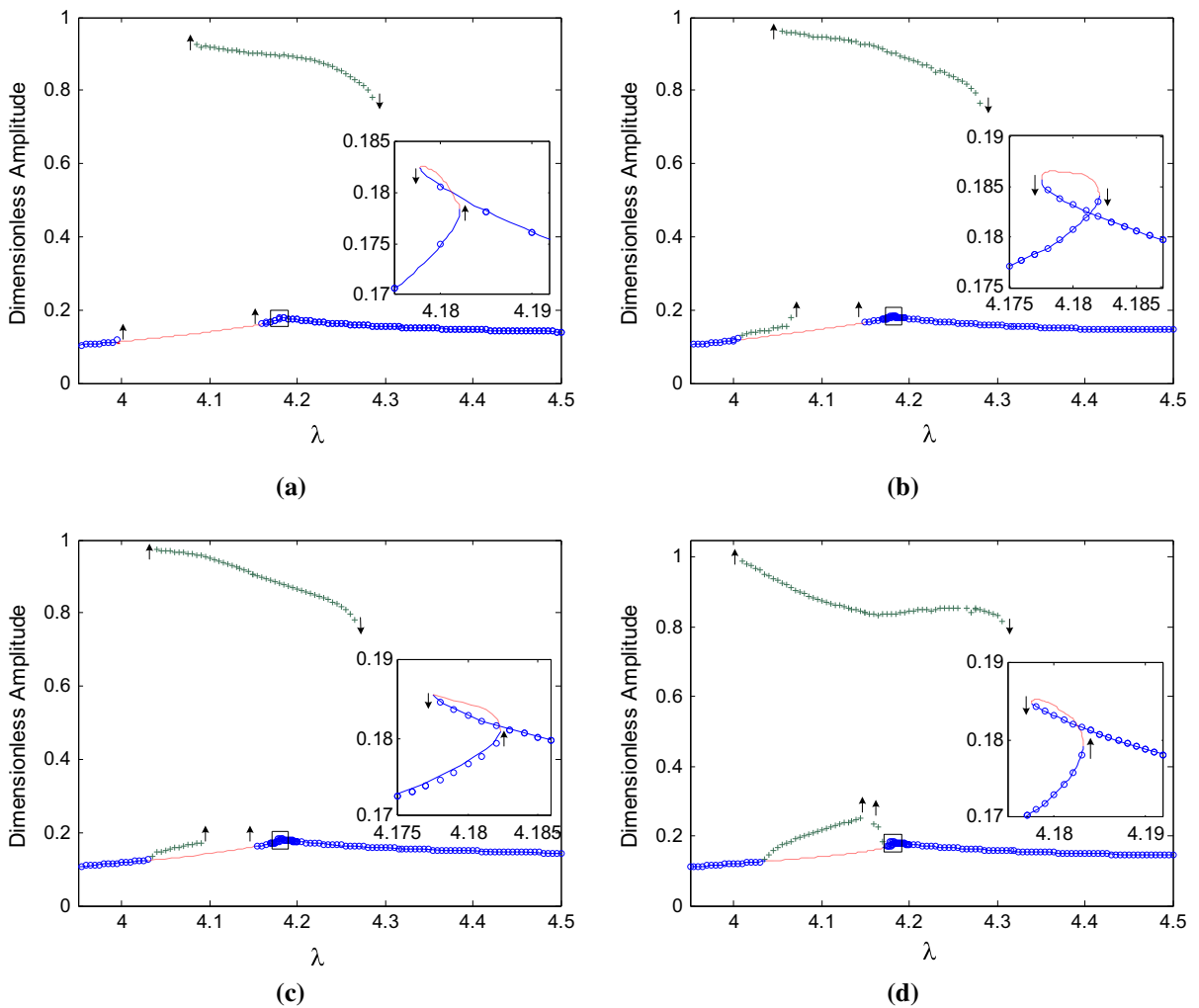

Fig. 11 Frequency–amplitude curves of resonance region with different frequency ratios. **a** $\xi = 1.25$, **b** $\xi = 1.28$, **c** $\xi = 1.30$, **d** $\xi = 1.33$. *Straight line* Harmonic balance (stable solution), *Dashed line* Harmonic balance (unstable solution), *Opencircle* Runge–Kutta (periodic solution), +Runge–Kutta (quasi-periodic solution)

decreases; meanwhile, the amplitude of combined frequency $2\omega_2 - \omega_1$ ascends sharply to reach the magnitude of amplitude of frequency ω_1. When λ goes near 0.75, the resonant peak is motivated by excitation of lower-frequency ω_1, and with the increase in the frequency ω_1, the amplitude of fundamental frequencies ω_1, ω_2 and combined frequency $2\omega_1 - \omega_2$ all increase. Out of the resonance region, the combined frequencies are all inconspicuous.

### 4.3 Resonance region of first bending mode

According to Fig. 2, the resonance region of first bending mode is another region which is worth analyzing the nonlinear characteristic. The response frequencies are shown in Fig. 8, it is obvious that the fundamental frequencies ω_1 and ω_2 are dominated and others combined frequencies are inconspicuous except frequencies $2\omega_1 - \omega_2$ and $3\omega_1 - 2\omega_2$.

As mentioned in Sect. 4.1, there exists quasi-periodic solutions in the resonance region, and Fig. 9 shows the solutions obtained by harmonic balance method and Runge-Kutta method. The points A, B are second Hopf bifurcation points, and the points C, D are saddle-node bifurcation points which are judged by the Floquet multipliers listed in Table 3, thus there are two unstable regions A-B and C-D on the periodic solution branch. The independent quasi-periodic solution

E-F exists in region from $\lambda = 4.040$ to $\lambda = 4.265$, coexisting with periodic solution, while quasi-periodic solution A-G comes from the unstable periodic solution. In the region between point C and point D, there are three solutions corresponded to one value of λ, for instance, Fig. 10 shows the comparison of the three solutions at $\lambda = 4.179$, ordered by amplitude from low to high, the first two solutions are periodic solutions, but the third one is a quasi-periodic solution.

The unstable solutions may lead to three different kinds of jump phenomena with the rotor speed going up or going down: between one quasi-periodic solution and another quasi-periodic solution, between quasi-periodic solution and periodic solution, and between two periodic solutions. When the rotor speed goes up through point A, the periodic solution loses stability entering the quasi-periodic motion, and with the increasing speed, the quasi-periodic motion on section A-G will jump up to the quasi-periodic section E-F, then jump down to the periodic solution. If the rotor speed goes up from point B, the periodic motion will go from point B to point C, and then jump up to another stable periodic solution with a small amplitude. When the rotor speed goes down, the periodic motion will jump down form point D and lose stability on point B resulting into periodic section E-F, the amplitude will become higher and higher until the computational divergence as the speed goes down. In this system, the resonant peak has the 'soft stiffness' char-

Fig. 12 Frequency–amplitude curves of resonance region with ratio $\xi = 1.36$
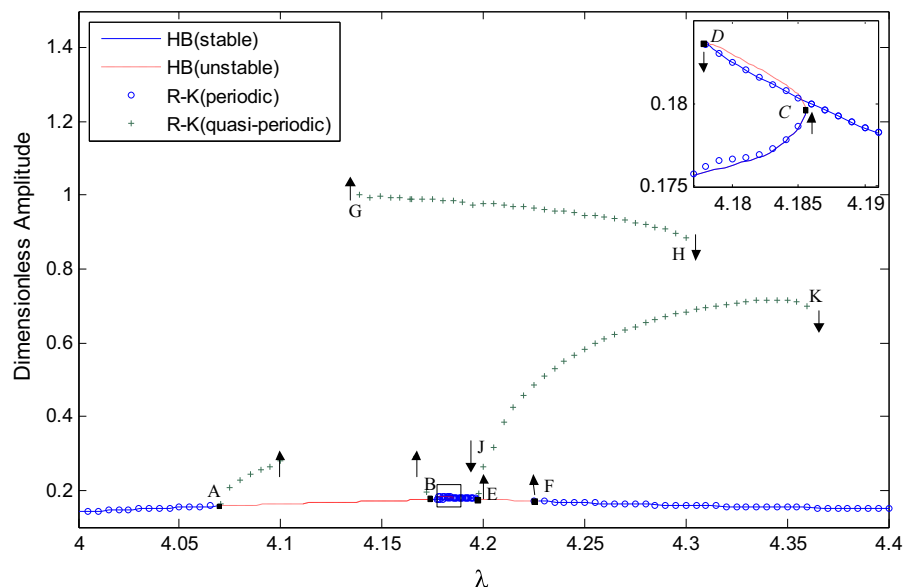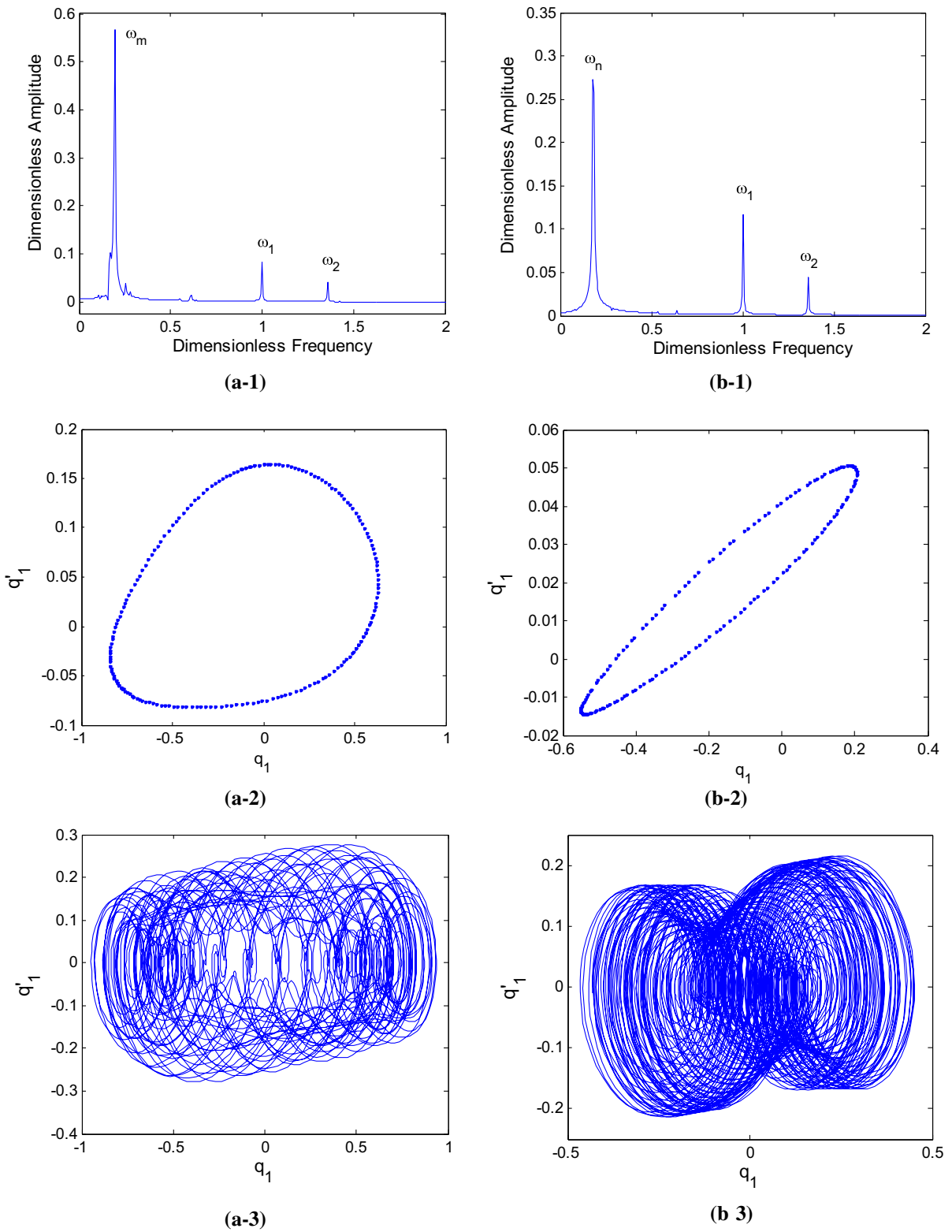
Fig. 13 Frequency spectrogram, Poincare section and phase diagram of two kinds of quasi-periodic solution at $\lambda = 4.25$ ($\xi = 1.36$)

acteristic, moreover, the multiple stable state solutions cause the large amplitude jump. The unstable section A-B is a main reason for the jump phenomenon, and the quasi-periodic solution E-F is an essential condition.

The unstable solution near the resonant peak of first bending mode was early reported by McLean and Hahn [28] in their study about a symmetry flexible rotor supported by squeeze film dampers under single excitation, and then Zhao [10] explained that the periodic solution loses stability through second Hopf bifurcation. In the study of single excitation system, Hussain [29] and Zhu [12], respectively, obtained the low amplitude quasi-periodic solution and the high amplitude quasi-periodic solution near the resonant peak of first bending mode, which are corresponding to the section AG and the section EF in this paper. Moreover, in this paper the resonant peak in the local figure of Fig. 9 forms a cross structure, and this characteristic was also reported in Zhu's work [12], thus it is a basic characteristic of nonlinear system consisted of SFD and flexible rotor.

The nonlinear characteristic such as second Hopf bifurcation, quasi-periodic solution and cross structure in this paper also can be obtained in flexible rotor-squeeze film dampers system with single excitation system, and the bifurcation mechanism and the region of quasi-periodic solution are agreed with the other researchers' results mentioned above.

4.4 Effect of parameters

The amplitude jump is a harmful effect on the system, and the unstable solution is an important factor of this phenomenon, so the effect of parameters on the unstable region should be analyzed.

Figure 11 shows the effect of ratio of excitation frequencies on unstable region and resonant peak. It is obvious that the quasi-periodic solution and unstable region are not distinct with the increase of the frequency ratio ξ, but the resonant peak shows the irregular change between 'soft spring characteristic' ($\xi = 1.25, \xi = 1.30, \xi = 1.33$) and a kind of 'cross characteristic' ($\xi = 1.28$).

Moreover, as shown in Fig. 12, when $\xi = 1.36$, besides the unstable region A-B and quasi-periodic solution G-H mentioned above, there is another unstable region E-F with quasi-periodic solution J-K. The points A, B, E, F are secondary Hopf bifurcation points, and points C, D are saddle-node bifurcation points. The jump phenomenon can occur from periodic solution to quasi-periodic solution or from quasi-periodic solution to quasi-periodic solution. Figure 13 shows the comparison of the two kinds of quasi-periodic solutions at $\lambda = 4.25$, it is clear to see the differences in the frequency spectrograms ($\omega_m = 0.195, \omega_n = 0.177$), Poincare sections and phase diagrams.

Figure 14 shows an interesting result in the case of $\xi = 1.37$, there are still two kinds of quasi-periodic
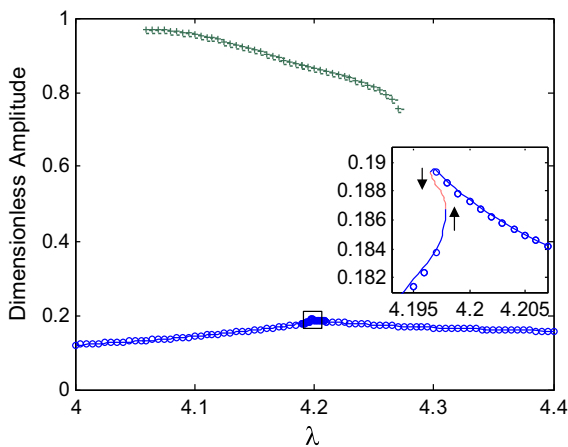

Fig. 14 Frequency–amplitude curves of resonance region with ratio $\xi = 1.37$
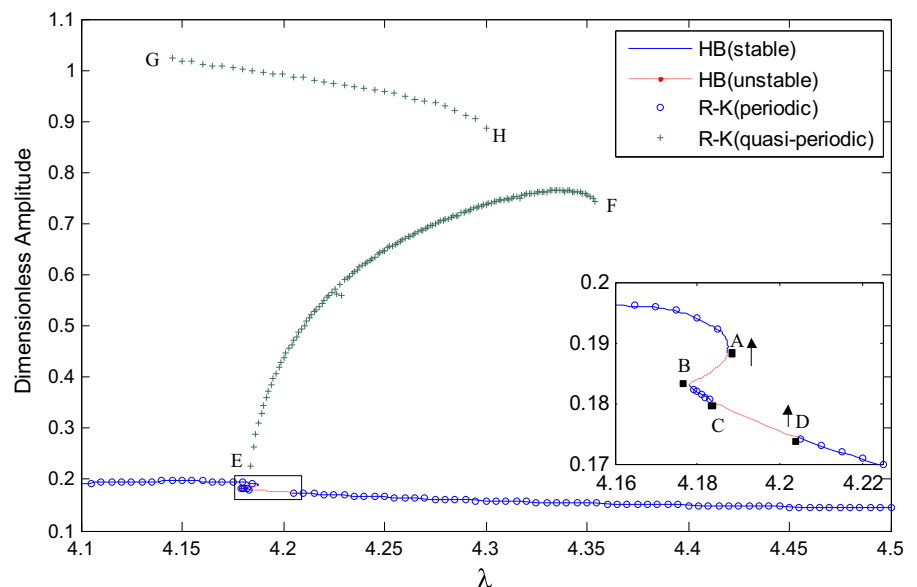
solutions, but unlike the results for $\xi = 1.36$, there are only two secondary Hopf bifurcation points C and D, and the unstable region at the left of resonant peak vanish. The resonant peak has the 'hard spring characteristic', but the periodic solution will jump from point A to the quasi-periodic solution E-F when the rotor speed goes up. Since the jump point *A* is beyond the unstable region C-D, the points B, C are saddle-node bifurcation points

The effects of the different ratios of excitation frequencies show abundant nonlinear phenomenon and multiple-solution conditions, and the system nonlinear characteristics are sensitive to the frequency ratio. The unstable solution caused by saddle-node bifurcation makes the cross structure of solution express the 'soft' or 'cross' characteristic: If the cross point is crossed by a unstable solution and a stable solution, the resonant peak has 'soft' characteristic; if the cross point is crossed by two stable solutions, the resonant peak has 'cross' characteristic. Moreover, the system also can express 'hard' characteristic in some other conditions.
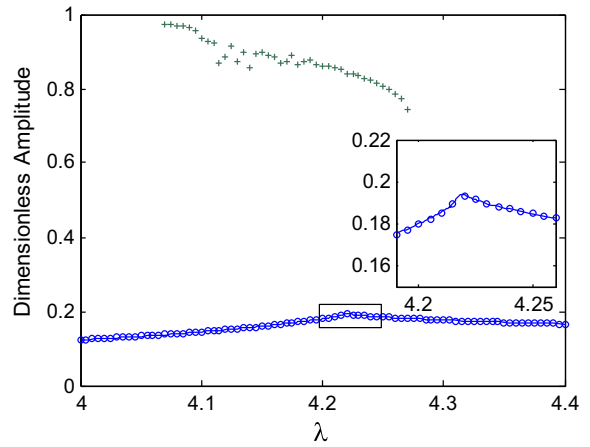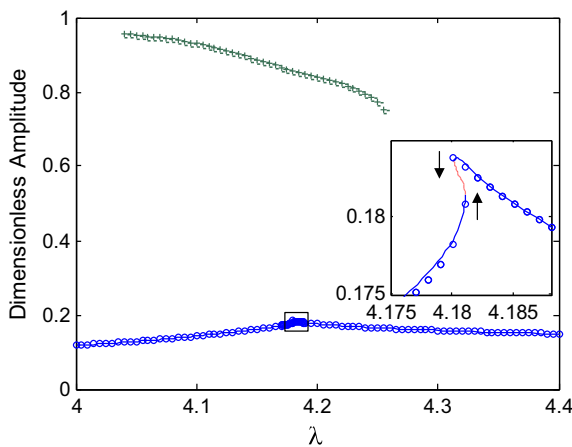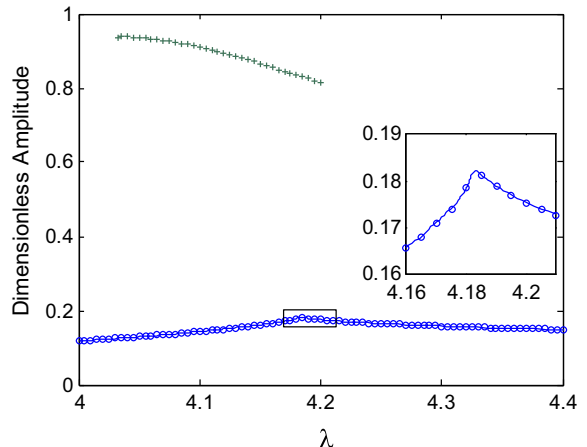
Fig. 15 Frequency–amplitude curves of resonance region with different parameters combination. **a** $c = 0.19$ mm, $\mu = 1.562 \times 10^{-2}$ N s/m^2, **b** $c = 0.18$ mm, $\mu = 1.562 \times 10^{-2}$ Ns/m^2, **c** $c = 0.20$ mm, $\mu = 1.708 \times 10^{-2}$ Ns/m^2, **d** $c = 0.20$ mm, $\mu = 1.855 \times 10^{-2}$ Ns/m^2. *Straight line* Harmonic balance (stable solution), *Dashed line* Harmonic balance (unstable solution), *opencircle* Runge-Kutta (periodic solution), +Runge-Kutta (quasi-periodic solution)

The effects of clearance c and kinetic viscosity coefficient μ under the same ratio $\xi = 1.3$ are shown in Fig. 15. Compared with Figs. 9 and 15a, b describe the effects of varying clearances on the system. The decrease of the clearance makes the cross structure vanish, makes the unstable region gradually disappear and leads to the periodic solutions of the region all be stable. Meanwhile, the quasi-periodic motions still exist, which may cause the jump phenomenon when the system receives some disturbance. Similarly, the increase in the viscosity can also attenuate the nonlinear characteristic as shown in Fig. 15c, d.

Summing up the above analysis, the basic nonlinear characteristic of flexible rotor combined with squeeze film damper under two-frequency excitations is similar to the system under single-frequency excitation, for instance, the jump phenomena and hard stiffness effect on the resonant peak of rigid body translation mode caused by saddle-node bifurcation, the jump phenomena nearby the resonant peak of the first bending mode caused by second Hopf bifurcation and independent quasi-periodic solution, and the cross structure on the resonant peak of the first bending mode caused by saddle-node bifurcation. The influence of SFD parameter is also similar to the single-frequency excitation system. However, the system with two-frequency excitations has its particular characteristic: The jump phenomena can exhibit different stiffness characteristics, i.e., 'soft', 'cross' and 'hard' due to different frequency ratio, and another unstable region and quasi-periodic solution could appear in certain frequency ratios; therefore, the frequency ratio is an important parameter in a two-frequency excited nonlinear system. Finally, the response of the combination frequencies is also a characteristic of two-frequency excited nonlinear system.

5 Conclusions

In this paper, the nonlinear characteristics of a flexible rotor with squeeze film damper excited by two-frequency excitation have been investigated via harmonic balance method and Runge-Kutta method. The nonlinear characteristics have been focused mainly on two resonance regions corresponding to the rigid body translation and first bending mode, respectively. It has been concluded that the responses in resonance region of rigid body translation perform jump phenomenon and show 'hard spring' nonlinear characteristic.

Besides the excitation frequencies, the response contains primary combination frequencies of $2\omega_2 - \omega_1$ and $2\omega_1 - \omega_2$. The response in resonance region of first bending mode has abundant nonlinear characteristic, for instance, jump phenomena caused by saddle-node bifurcation, second Hopf bifurcation and quasi-periodic solution, and the response contains primary combination frequencies of $2\omega_1 - \omega_2$ and $3\omega_1 - 2\omega_2$. The unstable solution caused by saddle-node bifurcation on the cross structure makes the resonant peak show 'soft' or 'cross' characteristics under different ratios of frequencies; moreover, the resonant peak also shows 'hard' characteristic in the case of $\xi = 1.37$. The unstable solution caused by secondary Hopf bifurcation makes the system perform quasi-periodic motions and jump up to other independent quasi-periodic motions with large amplitudes. In some conditions ($\xi = 1.36$, $\xi = 1.37$), there are two independent quasi-periodic solutions, the system shows more complex jump phenomenon. The number of unstable regions and the nonlinear characteristics are sensitive to the ratio of excitation frequencies. The decrease in clearance or increase in viscosity could attenuate the nonlinear characteristics of resonant peak. The results in the paper will contribute to a better understanding of the nonlinear dynamic behaviors of the SFD-rotor systems with two excitations and provide a theoretical foundation for optimization of the system parameters.

Appendix 1: List of symbols

$a_{j,k,l}, b_{j,k,l}$	Harmonic coefficients of dimensionless displacements, dimensionless
A	Periodic matrix, dimensionless
B	Dimensionless bearing parameter of squeeze film damper, dimensionless
c	Clearance of squeeze film damper, m
$c_{j,k,l}, d_{j,k,l}$	Harmonic coefficients of dimensionless nonlinear forces, dimensionless
c_1	Damping coefficient corresponding to transverse deformation of the shaft, N s/m

c_2, c_3	Damping coefficients corresponding to coupling deformation of the shaft, N s	N	Number of discrete points in time domain, dimensionless
c_4	Damping coefficient corresponding to angular deformation of the shaft, N m s	P	Vector of harmonic coefficients of dimensionless displacements, dimensionless
c_5, c_6	Damping coefficients of the supports, N s/m	q_j	Dimensionless displacement (j=1∼8), dimensionless
D	Monodromy matrix, dimensionless	Q	Vector of harmonic coefficients of dimensionless nonlinear forces, dimensionless
F_{cx}, F_{cy}	Oil film forces in the Cartesian coordinate system, N		
$\bar{F}_{cx}, \bar{F}_{cy}$	Dimensionless oil film forces in the Cartesian coordinate system, dimensionless	r	Radial displacement of journal, m
		R	Radius of the journal, m
F_r, F_τ	Oil film forces in the polar coordinate system, N	s	Dimensionless arc length, dimensionless
$\bar{F}_r, \bar{F}_\tau$	Dimensionless oil film forces in the polar coordinate system, dimensionless	t	Time, s
		U	Vector of state variables, dimensionless
G	Vector of harmonic balance terms, dimensionless	U_1, U_2, U_3	Dimensionless unbalance value, dimensionless
J	Jacobi matrix, dimensionless	x, y	Displacements of center of disk, m
J_d	Equivalent equatorial moment of inertia of the disk, kg m^2	x_a, y_a	Displacements of center of left journal, m
J_p	Equivalent polar moment of inertia of the disk, kg m^2	x_b, y_b	Displacements of center of right journal, m
k, l	Harmonic parameters, dimensionless	$\alpha_0, \alpha_1, \alpha_2$	Dimensionless mass, dimensionless
k_{rr}	Stiffness coefficient corresponding to transverse deformation of the shaft, N/m	γ_1, γ_2	Ratio of distance l_1, l_2 to length l, dimensionless
$k_{r\varphi}, k_{\varphi r}$	Stiffness coefficients corresponding to coupling deformation of the shaft, N	δ_1, δ_2	Unbalance value, kg m
$k_{\varphi\varphi}$	Stiffness coefficient corresponding to angular deformation of the shaft, N m	ε	Dimensionless radial displacement of journal, dimensionless
k_a, k_b	Stiffness coefficient of the supports, N/m	ζ_j	Dimensionless damping coefficients (j=1∼6), dimensionless
l	Length of the shaft, m	η	Ratio of moment of inertia J_p to moment of inertia J_d, dimensionless
l_1	Distance from the disk to the left support, m		
l_2	Distance from the disk to the right support, m	θ	Journal position angle measured from line of journal centers, dimensionless
l_3	Distance from the disk to the intershaft bearing, m	θ_1, θ_2	Angles from line of journal centers to start and end of positive pressure region, dimensionless
L	Length of squeeze film damper, m	θ_x, θ_y	Angles of disk rotate along x axis and y axis, dimensionless
m, n	Parameters of discrete points in time domain, dimensionless	κ_j	Dimensionless stiffness coefficients (j=1∼6), dimensionless
m_o	Equivalent mass of the rotor, kg	λ	Bifurcation parameter, dimensionless
m_a	Equivalent mass of the left journal, kg	μ	Viscosity coefficient of oil, N s/m^2
m_b	Equivalent mass of the right journal, kg	ξ	Ratio of high excitation frequency Ω_2 to low excitation frequency Ω_1, dimensionless
M	Maximal harmonic parameter, dimensionless		
		τ, τ_1, τ_2	Dimensionless time, dimensionless

ψ	angular displacement of journal, dimensionless
ω_1, ω_2	Dimensionless low excitation frequency and dimensionless high excitation frequency, dimensionless
Ω_0	Reference rotational speed
Ω_1, Ω_2	Low-pressure rotor rotational speed and high-pressure rotor rotational speed, rad/s

Appendix 2

$$g_{3,k,l} = \left[\kappa_1 - (k+l\xi)^2\right] a_{2kl} + \zeta_1 (k+l\xi) b_{2kl}$$
$$+ \kappa_2 a_{3kl} + \zeta_2 (k+l\xi) b_{3kl} - (\kappa_2 + \gamma_2\kappa_1) a_{6kl}$$
$$- (\zeta_2 + \gamma_2\zeta_1)(k+l\xi) b_{6kl} + (\kappa_2 - \gamma_1\kappa_1) a_{8kl}$$
$$+ (\zeta_2 - \gamma_1\zeta_1)(k+l\xi) b_{8kl} = 0$$

$$g_{4,k,l} = -\zeta_1 (k+l\xi) a_{2kl} + \left[\kappa_1 - (k+l\xi)^2\right] b_{2kl}$$
$$- \zeta_2 (k+l\xi) a_{3kl} + \kappa_2 b_{3kl} + (\zeta_2 + \gamma_2\zeta_1)(k+l\xi) a_{6kl}$$
$$- (\kappa_2 + \gamma_2\kappa_1) b_{6kl} - (\zeta_2 - \gamma_1\zeta_1)(k+l\xi) a_{8kl}$$
$$+ (\kappa_2 - \gamma_1\kappa_1) b_{8kl} - U_1\phi_1 - \xi^2 U_2\phi_2 = 0$$

$$g_{5,k,l} = \kappa_3 a_{2kl} + \zeta_3 (k+l\xi) b_{2kl} + \left[\kappa_4 - \alpha_0 (k+l\xi)^2\right] a_{3kl}$$
$$+ \zeta_4 (k+l\xi) b_{3kl} + \alpha_0\eta (k+l\xi) b_{4kl}$$
$$- (\kappa_4 + \gamma_2\kappa_3) a_{6kl}$$
$$- (\zeta_4 + \gamma_2\zeta_3)(k+l\xi) b_{6kl} + (\kappa_4 - \gamma_1\kappa_3) a_{8kl}$$
$$+ (\zeta_4 - \gamma_1\zeta_3)(k+l\xi) b_{8kl} = 0$$

$$g_{6,k,l} = -\zeta_3 (k+l\xi) a_{2kl} + \kappa_3 b_{2kl} - \zeta_4 (k+l\xi) a_{3kl}$$
$$+ \left[\kappa_4 - \alpha_0 (k+l\xi)^2\right] b_{3kl} - \alpha_0\eta (k+l\xi) a_{4kl}$$
$$+ (\zeta_4 + \gamma_2\zeta_3)(k+l\xi) a_{6kl} - (\kappa_4 + \gamma_2\kappa_3) b_{6kl}$$
$$- (\zeta_4 - \gamma_1\zeta_3)(k+l\xi) a_{8kl} + (\kappa_4 - \gamma_1\kappa_3) b_{8kl}$$
$$- \xi^2 U_3\phi_2 = 0$$

$$g_{7,k,l} = -\kappa_3 a_{1kl} - \zeta_3 (k+l\xi) b_{1kl} - \alpha_0\eta (k+l\xi) b_{3kl}$$
$$+ \left[\kappa_4 - (k+l\xi)^2\right] a_{4kl} + \zeta_4 (k+l\xi) b_{4kl}$$
$$+ (\kappa_4 + \gamma_2\kappa_3) a_{5kl} + (\zeta_4 + \gamma_2\zeta_3)(k+l\xi) b_{5kl}$$
$$- (\kappa_4 - \gamma_1\kappa_3) a_{7kl} - (\zeta_4 - \gamma_1\zeta_3)(k+l\xi) b_{7kl}$$
$$+ \xi^2 U_3\phi_2 = 0$$

$$g_{8,k,l} = \zeta_3 (k+l\xi) a_{1kl} - \kappa_3 b_{1kl} + \alpha_0\eta (k+l\xi) a_{3kl}$$
$$- \zeta_4 (k+l\xi) a_{4kl} + \left[\kappa_4 - (k+l\xi)^2\right] b_{4kl}$$
$$- (\zeta_4 + \gamma_2\zeta_3)(k+l\xi) a_{5kl} + (\kappa_4 + \gamma_2\kappa_3) b_{5kl}$$
$$+ (\zeta_4 - \gamma_1\zeta_3)(k+l\xi) a_{7kl} - (\kappa_4 - \gamma_1\kappa_3) b_{7kl} = 0$$

$$g_{9,k,l} = -\gamma_2\kappa_1 a_{1kl} - \gamma_2\zeta_1 (k+l\xi) b_{1kl} + \gamma_2\kappa_2 a_{4kl} + \gamma_2\zeta_2$$
$$(k+l\xi) b_{4kl} + \left[\left(\kappa_5 + \gamma_2\kappa_2 + \gamma_2^2\kappa_1\right) - \alpha_1 (k+l\xi)^2\right] a_{5kl}$$

$$+ \left[\zeta_5 + \gamma_2 (\zeta_2 + \gamma_2\zeta_1)\right](k+l\xi) b_{5kl} - \gamma_2 (\kappa_2 - \gamma_1\kappa_1)$$
$$a_{7kl} - \gamma_2 (\zeta_2 - \gamma_1\zeta_1)(k+l\xi) b_{7kl} + Bc_{5kl} = 0$$

$$g_{10,k,l} = \gamma_2\zeta_1 (k+l\xi) a_{1kl} - \gamma_2\kappa_1 b_{1kl} - \gamma_2\zeta_2 (k+l\xi) a_{4kl}$$
$$+ \gamma_2\kappa_2 b_{4kl} - \left[\gamma_2 (\zeta_2 + \gamma_2\zeta_1) + \zeta_5\right](k+l\xi) a_{5kl}$$
$$+ \left[\left(\kappa_5 + \gamma_2\kappa_2 + \gamma_2^2\kappa_1\right) - \alpha_1 (k+l\xi)^2\right] b_{5kl}$$
$$- \gamma_2 (\kappa_2 - \gamma_1\kappa_1) b_{7kl} + \gamma_2 (\zeta_2 - \gamma_1\zeta_1)(k+l\xi) a_{7kl}$$
$$+ Bd_{5kl} = 0$$

$$g_{11,k,l} = -\gamma_2\kappa_1 a_{2kl} - \gamma_2\zeta_1 (k+l\xi) b_{2kl}$$
$$- \gamma_2\kappa_2 a_{3kl} - \gamma_2\zeta_2 (k+l\xi) b_{3kl}$$
$$+ \left[\left(\kappa_5 + \gamma_2\kappa_2 + \gamma_2^2\kappa_1\right) - \alpha_1 (k+l\xi)^2\right] a_{6kl}$$
$$+ \left[\zeta_5 + \gamma_2 (\zeta_2 + \gamma_2\zeta_1)\right](k+l\xi) b_{6kl}$$
$$- \gamma_2 (\kappa_2 - \gamma_1\kappa_1) a_{8kl} - \gamma_2 (\zeta_2 - \gamma_1\zeta_1)(k+l\xi) b_{8kl}$$
$$+ Bc_{6kl} = 0$$

$$g_{12,k,l} = \gamma_2\zeta_1 (k+l\xi) a_{2kl} - \gamma_2\kappa_1 b_{2kl}$$
$$+ \gamma_2\zeta_2 (k+l\xi) a_{3kl}$$
$$- \gamma_2\kappa_2 b_{3kl} - \left[\gamma_2 (\zeta_2 + \gamma_2\zeta_1) + \zeta_5\right](k+l\xi) a_{6kl}$$
$$+ \left[\left(\kappa_5 + \gamma_2\kappa_2 + \gamma_2^2\kappa_1\right) - \alpha_1 (k+l\xi)^2\right] b_{6kl}$$
$$+ \gamma_2 (\zeta_2 - \gamma_1\zeta_1)(k+l\xi) a_{8kl} - \gamma_2 (\kappa_2 - \gamma_1\kappa_1) b_{8kl}$$
$$+ Bd_{6kl} = 0$$

$$g_{13,k,l} = -\gamma_1\kappa_1 a_{1kl} - \gamma_1\zeta_1 (k+l\xi) b_{1kl}$$
$$+ \gamma_1\kappa_2 a_{4kl} + \gamma_1\zeta_2 (k+l\xi) b_{4kl} + \gamma_1 (\kappa_2 + \gamma_2\kappa_1) a_{5kl}$$
$$+ \gamma_1 (\zeta_2 + \gamma_2\zeta_1)(k+l\xi) b_{5kl}$$
$$+ \left[\left(\kappa_6 - \gamma_1\kappa_2 + \gamma_1^2\kappa_1\right) - \alpha_2 (k+l\xi)^2\right] a_{7kl}$$
$$+ \left[\gamma_1 (-\zeta_2 + \gamma_1\zeta_1) + \zeta_6\right](k+l\xi) b_{7kl} = 0$$

$$g_{14,k,l} = \gamma_1\zeta_1 (k+l\xi) a_{1kl} - \gamma_1\kappa_1 b_{1kl}$$
$$- \gamma_1\zeta_2 (k+l\xi) a_{4kl}$$
$$+ \gamma_1\kappa_2 b_{4kl} - \gamma_1 (\zeta_2 + \gamma_2\zeta_1)(k+l\xi) a_{5kl}$$
$$+ \gamma_1 (\kappa_2 + \gamma_2\kappa_1) b_{5kl}$$
$$+ \left[\left(\kappa_6 - \gamma_1\kappa_2 + \gamma_1^2\kappa_1\right) - \alpha_2 (k+l\xi)^2\right] b_{7kl}$$
$$- \left[\gamma_1 (-\zeta_2 + \gamma_1\zeta_1) + \zeta_6\right](k+l\xi) a_{7kl} = 0$$

References

1. Cooper, S.: Preliminary investigation of oil films for the control of vibration. In: Proceedings of the Lubrication and Wear Convention, pp. 305–315. Institution of Mechanical Engineers (1963)
2. Mohan, S., Hahn, E.J.: Design of squeeze film damper supports for rigid rotors. ASME J. Manuf. Sci. Eng. **96**(3), 976–982 (1974)

3. Levesley, M.C., Holmes, R.: The efficient computation of the vibration response of an aero-engine rotor-damper assembly. Proc. Inst. Mech. Eng. Part G: J. Aerosp. Eng. **208**(1), 41–51 (1994)

4. Taylor, D.L., Kumar, B.R.K.: Nonlinear response of short squeeze film dampers. ASME J. Tribol. **102**(1), 51–58 (1980)

5. Gunter, E.J., Barrett, L.E., Allaire, P.E.: Design of nonlinear squeeze-film dampers for aircraft engines. ASME J. Tribol. **99**(1), 57–64 (1977)

6. Zeidan, F., Vance, J.: Cavitation and air entrainment effects on the response of squeeze film supported rotors. ASME J. Tribol. **112**(2), 347–353 (1990)

7. Nikolajsen, J.L., Holmes, R.: Investigation of squeeze-film isolators for the vibration control of a flexible rotor. Proc. Inst. Mech. Eng. Part C: J. Mech. Eng. Sci. **21**(4), 247–252 (1979)

8. Holmes, R., Dogan, M.: Investigation of a rotor bearing assembly incorporating a squeeze-film damper bearing. Proc. Inst. Mech. Eng. Part C: J. Mech. Eng. Sci. **24**(3), 129–137 (1982)

9. Sykes, J.E.H., Holmes, R.: The effects of bearing misalignment on the non-linear vibration of aero-engine rotor-damper assemblies. Proc. Inst. Mech. Eng. Part G: J. Aerosp. Eng. **204**(2), 83–99 (1990)

10. Zhao, J.Y., Linnett, I.W., McLean, L.J.: Stability and bifurcation of unbalanced response of a squeeze film damped flexible rotor. ASME J. Tribol. **116**(2), 361–368 (1994)

11. Zhao, J.Y., Linnett, I.W., McLean, L.J.: Subharmonic and quasi-periodic motions of an eccentric squeeze film damper-mounted rigid rotor. ASME J. Vib. Acoust. **116**(3), 357–363 (1994)

12. Zhu, C.S., Robb, D.A., Ewins, D.J.: Analysis of the multiple-solution response of a flexible rotor supported on non-linear squeeze film dampers. J. Sound Vib. **252**, 389–408 (2002)

13. Sundararajan, P., Noah, S.T.: Dynamics of forced nonlinear systems using shooting/arc-length continuation method–application to rotor systems[J]. ASME J. Vib. Acoust. **119**(1), 9–20 (1997)

14. Inayat-Hussain, J.I., Kanki, H., Mureithi, N.W.: On the bifurcations of a rigid rotor response in squeeze-film dampers. J. Fluids Struct. **17**, 433–459 (2003)

15. Inayat-Hussain, J.I., Kanki, H., Mureithi, N.W.: Chaos in the unbalance response of a rigid rotor in cavitated squeeze-film dampers without centering springs. Chaos Soliton Fract. **13**(4), 929–945 (2002)

16. Bonello, P., Brennan, M.J., Holmes, R.: Non-linear modelling of rotor dynamic systems with squeeze film dampers—an efficient integrated approach. J. Sound Vib. **249**(4), 743–773 (2002)

17. Chang-Jian, C.W., Kuo, J.K.: Bifurcation and chaos for porous squeeze film damper mounted rotor-bearing system lubricated with micropolar fluid. Nonlinear Dyn. **58**(4), 697–714 (2009)

18. Boyaci, A., Lu, D., Schweizer, B.: Stability and bifurcation phenomena of Laval/Jeffcott rotors in semi-floating ring bearings. Nonlinear Dyn. **79**(2), 1535–1561 (2015)

19. Schweizer, B.: Oil whirl, oil whip and whirl/whip synchronization occurring in rotor systems with full-floating ring bearings. Nonlinear Dyn. **57**(4), 509–532 (2009)

20. Zhou, H.L., Luo, G.H., Chen, G., et al.: Analysis of the nonlinear dynamic response of a rotor supported on ball bearings with floating-ring squeeze film dampers. Mech. Mach. Theory **59**, 65–77 (2013)

21. Hai, P.M., Bonello, P.: An impulsive receptance technique for the time domain computation of the vibration of a whole aero-engine model with nonlinear bearings. J. Sound Vib. **318**(3), 592–605 (2008)

22. Bonello, P., Hai, P.M.: Computational studies of the unbalance response of a whole aero-engine model with squeeze-film bearings. ASME J. Eng. Gas Turbines Power **132**(3), 032504 (2010)

23. Bonello, P., Pham, H.M.: A theoretical and experimental investigation of the dynamic response of a squeeze-film damped twin-shaft test rig. Proc. Inst. Mech. Eng. Part C: J. Mech. Eng. Sci. **228**(2), 218–229 (2014)

24. Booker, J.F.: A table of the journal bearing integral. ASME J. Basic Eng. **87**(2), 533–535 (1965)

25. Kim, Y.B., Choi, S.K.: A multiple harmonic balance method for the internal resonant vibration of a non-linear Jeffcott rotor. J. Sound Vib. **208**(5), 745–761 (1997)

26. Zhang, Z.Z., Chen, Y.S., Cao, Q.J.: Bifurcations and hysteresis of varying compliance vibrations in the primary parametric resonance for a ball bearing. J. Sound Vib. **350**, 171–184 (2015)

27. Hsu, C.S.: On approximating a general linear periodic system. J. Math. Anal. Appl. **45**(1), 234–251 (1974)

28. McLean, L.J., Hahn, E.J.: Stability of squeeze film damped multi-mass flexible rotor bearing systems. ASME J. Tribol. **107**(3), 402–409 (1985)

29. Inayat-Hussain, J.I.: Bifurcations in the response of a flexible rotor in squeeze-film dampers with retainer springs. Chaos Soliton Fract. **39**(2), 519–532 (2009)